Acta Crystallographica Section D
Biological Crystallography
ISSN 0907-4449

Purification, crystallization and preliminary X-ray analysis of the GTP-binding protein Rab9 implicated in endosome-to-TGN vesicle trafficking

Julia G. Wittmann and Markus G. Rudolph*

Molecular Structural Biology, University of Göttingen, Justus-von-Liebig-Weg 11, Göttingen D-37077, Germany

Correspondence e-mail: markus.rudolph@bio.uni-goettingen.de

Received 16 December 2003
Accepted 13 January 2004

Rab GTP-binding proteins are involved in the regulation of distinct vesicular-transport events involving membrane targeting and fusion. They differ from other small GTPases by the presence of specific loop regions that serve as effector-binding sites in addition to the classical switch I and switch II regions. While the structures of many small GTP-binding proteins of the Ras superfamily are available in both GDP- and GTP-bound forms, Rab proteins are less well characterized than Ras proteins at the structural level. The crystallization of Rab9, a key regulatory component in the recycling of mannose-6-phosphate receptors from endosomes to the trans-Golgi network, is described here.

1. Introduction

Transport of proteins between different compartments in eukaryotic cells during exocytosis, endocytosis, transcytosis and secretion is mediated by vesicles that bud from a donor compartment and fuse with the membrane of an acceptor compartment (Segev, 2001). During anterograde transport, cargo proteins in the endoplasmic reticulum (ER) or Golgi need to be sorted correctly into budding vesicles, which are targeted to their specific acceptor compartments, such as the cell membrane or endosomes. Signal sequences on the cargo proteins are recognized by membrane-spanning receptors in the donor compartment to ensure correct targeting. Retrieval of these receptors during retrograde transport from the acceptor compartment to the Golgi or ER is regulated in order to keep anterograde and retrograde transport in equilibrium and to maintain compartment morphology. These processes are regulated by small Ras-like GTP-binding proteins of the Ypt/Rab family, about 60 of which have been identified in mammals (Pfeffer, 2001). Similarly to other Ras-like GTPases, Rab (named after Ras genes from rat brain) proteins serve as molecular switches that cycle between an inactive GDP-bound and an active GTP-bound state, the ratio of which is regulated by specific GTPase-activating proteins (GAPs) and guanine nucleotide-exchange factors (GEFs; Vetter & Wittinghofer, 2001).

Rab9 has been identified as a key regulatory factor in the retrograde transport of mannose-6-phosphate receptors (MPR) from late endosomes to the trans-Golgi network mediated by TIP47 (Diaz & Pfeffer, 1998; Carroll *et al.*, 2001). However, no structural information about Rab9 is available. This is the first report describing crystals of the Rab9–GDP complex and thus establishing a basis for further structural characterization of this important regulatory pathway.

2. Experimental procedures and results

2.1. Cloning, expression and purification

A C-terminally truncated fragment coding for residues 1–175 (19.9 kDa) of Rab9 from *Canis familiaris* (GenBank accession No. X56386), which is identical in sequence to the human Rab9 protein, was PCR cloned using primers 5′-GGCCCATGGCAGGAAAATCTTCACTTTTTAAAG-3′ and 5′-GGCCTCGAGTCAAGTAGCAAGCACTCTTCGAACAGCTTC-3′ into the *Nco*I/*Xho*I restriction sites of pETM-30 (G. Stier, EMBL Heidelberg). This modified pET vector allows production of a His_6-GST-fusion protein (GST is glutathione-*S*-transferase) containing a tobacco etch virus (TEV) protease site after the GST part. The plasmid was transformed into *Escherichia coli* BL21 (DE3) RIL (Stratagene) and overproduction of the fusion protein was induced at an OD_{600} of 0.6 with 0.1 m*M* IPTG at 310 K for 4 h. Cells were harvested by centrifugation, resuspended in 50 m*M* Tris–HCl pH 7.5, 500 m*M* NaCl and 5 m*M* $MgCl_2$ and disrupted in a fluidizer (Microfluidics). The supernatant after centrifugation was applied onto a glutathione (GSH) Sepharose column (Amersham) equilibrated with 50 m*M* Tris–HCl pH 7.5, 100 m*M* NaCl and 5 m*M* $MgCl_2$. The GST-fusion protein was eluted in buffer supplemented with 20 m*M* GSH and cleaved overnight with TEV protease. Ni^{2+}–NTA agarose affinity chromatography (Qiagen) was used to separate His_6-GST and non-cleaved fusion protein from Rab9. The flowthrough containing Rab9 was concentrated and applied to an S75 size-exclusion column (Amersham)

equilibrated in 20 m*M* HEPES–NaOH pH 7.4 and 5 m*M* $MgCl_2$. Prior to crystallization, the protein was concentrated by ultrafiltration to 20 mg ml^{-1}. The final yield was ~2 mg per litre of *E. coli* culture. The presence of 100% GDP was assessed by analytical HPLC as described by Tucker *et al.* (1986).

Table 1
Crystallographic data collection and analysis.

Values in parentheses correspond to the highest resolution shell. The trigonal data set was scaled in *P*3 and *P*321.

Data set	*I*4	*P*3/*P*321
Source	PSF BL1	PSF BL1
Detector	MAR CCD 165	MAR CCD 165
Temperature (K)	100	100
Wavelength (Å)	0.9184	0.9184
Unit-cell parameters (Å)	a = 99.5, c = 79.8	a = 76.8, c = 189.8
V_M (Å^3 Da^{-1})	2.6	2.7
No. molecules in AU	2	6/3
Resolution (Å)	50–1.86 (1.93–1.86)	50.0–3.0 (3.11–3.00)
Measured reflections	105386	31948/32081
Unique reflections	28262	16484/10183
Mosaicity (°)	0.5	0.9
R_{sym} (%)	8.1 (25.4)	5.5 (45.2)/5.9 (48.4)
Completeness (%)	88.3 (31.3)	65.6 (45.0)/74.5 (53.5)
Average $I/\sigma(I)$	42.3 (2.0)	13.4 (1.9)/16.4 (2.3)

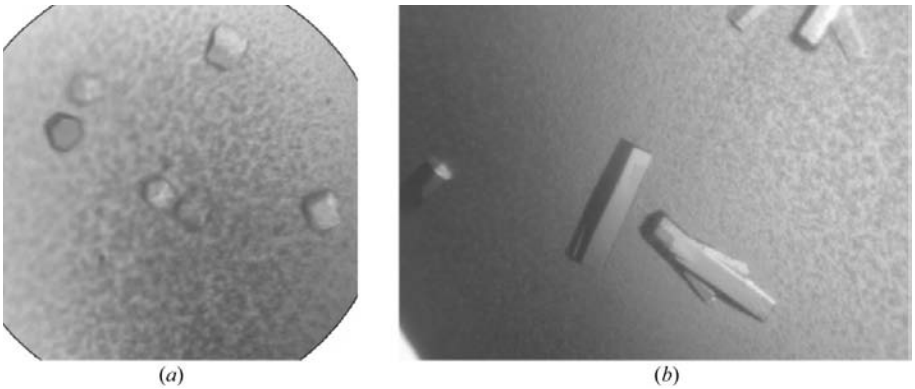

Figure 1
Tetragonal (*a*) and trigonal (*b*) crystals of the Rab9–GDP complex. The largest dimension is ~0.15 mm for the tetragonal crystals and ~0.3 mm for the trigonal crystals.

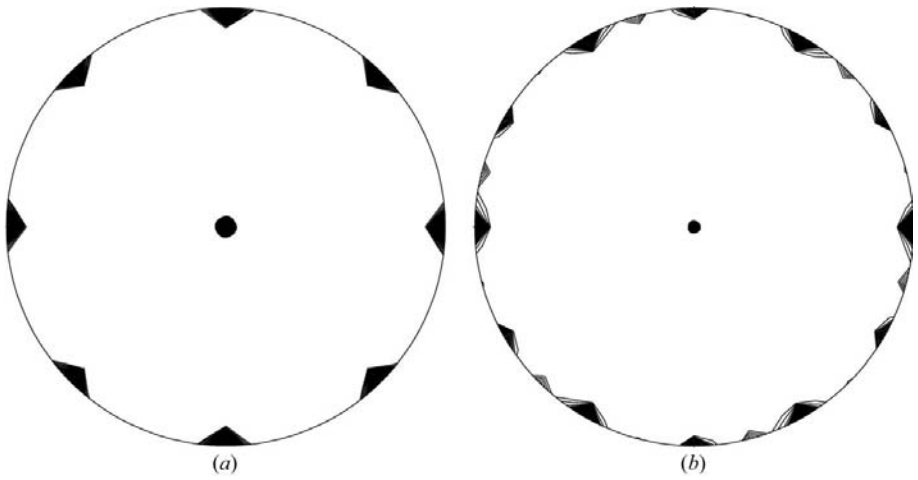

Figure 2
Self-rotation function plot of the $\kappa = 180°$ section of data processed in *I*4 (*a*) and *P*3 (*b*). The fourfold axis in the tetragonal crystal form is manifested by the peak at $\omega = 0°$ at the centre. Pseudo-422 symmetry ($\omega = 90°$ at the perimeter, $\varphi = 0$ and 45°) is introduced by non-crystallographic symmetry and/or twinning, the twin operator being a twofold rotation about the *b* axis. The same section of the self-rotation function in the trigonal crystal form shows highest peaks at $\omega = 90°$, $\varphi = 0$ or 60°, indicating *P*321 symmetry or a translation thereof. Weaker peaks of 65% of the maximum peak height are visible at $\omega = 0°$ as well as $\omega = 90°$, $\varphi = 30°$ and $\omega = 90°$, $\varphi = 90°$, which is unexpected for *P*321 but possible as a result of introduction of pseudo-622 symmetry by twinning. Other peaks at $\omega = 90°$ may arise from non-crystallographic symmetry.

2.2. Crystallization

Lead conditions were found by screening around the published crystallization conditions of other small GTP-binding proteins. Small crystals of Rab9–GDP grew overnight in the sitting-drop setup over a range of 16–22% PEG 8000 with various salts as co-precipitants. A fine screen established sodium benzoate as the best co-precipitant on the basis of crystal size and habit (tetragonal or hexagonal; Fig. 1). Diffraction-quality crystals grew within 2 d at 295 K from 1:1 mixtures of Rab9–GDP and reservoir containing 18.5% PEG 8000, 0.1 *M* MES–NaOH pH 6.0, 0.2 *M* sodium benzoate, 5 m*M* $MgCl_2$ and 2% ethanol for the hexagonal crystal form, and 18.5% PEG 8000, 0.1 *M* MES–NaOH pH 6.0, 0.2 *M* sodium benzoate, 5 m*M* $MgCl_2$, 2% ethanol and 8 m*M* $SrCl_2$ for the tetragonal crystal form. While variation of the alcohol did not change the crystal habit, the addition of $SrCl_2$ to the mother liquor was found to be responsible for the change in crystal shape from hexagonal to tetragonal, indicating specific binding of Sr^{2+} (see below).

2.3. Data collection and analysis

Prior to data collection, crystals were cryoprotected by a 20–30 s soak in mother liquor containing 20% ethylene glycol and vitrified in a 100 K N_2 stream. Data from both tetragonal and hexagonal shaped crystals were collected at beamline BL-1 of the Berliner Elektronenspeicherring für Synchrotronstrahlung (BESSY; Table 1) and reduced with the *HKL* suite of programs (Otwinowski & Minor, 1997). Indexing of the data suggested an *I*-centred tetragonal and a primitive trigonal lattice, respectively, for the two crystal morphologies. Systematic absences in the data from the tetragonal crystal form clearly showed the presence of a screw axis along *c*, establishing space group $I4_1$ (or $I4_122$, see below) for this crystal.

Self-rotation function analysis using *POLARRFN* (Collaborative Computational Project Number 4, 1994) of data sets reduced in *I*4 and *P*3 showed additional symmetry elements consistent with a higher metric symmetry in both cases, *i.e.* *I*422 instead of *I*4 and *P*321 or even *P*622 instead of *P*3 (Fig. 2). Further analysis of the intensity distributions using *TRUNCATE* and *DETWIN* (Collaborative Computational Project, Number 4, 1994) strongly suggested the presence of hemihedral twinning in both crystal forms, with a twin frac-

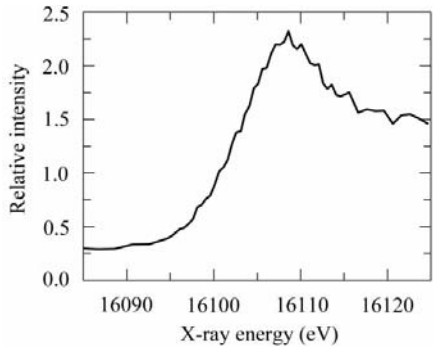

Figure 3
The emission scan of a tetragonal Rab9 crystal near the Sr *K* edge displays a peak at 16.104 KeV, confirming the presence of Sr.

tion close to 0.5 (data not shown). Thus, the additional symmetry elements observed in the self-rotation functions are probably a result of twinning. No off-origin peaks were visible in native Patterson maps, excluding the presence of pseudo-translational symmetry.

The addition of $SrCl_2$ to the crystallization mother liquor yielded tetragonal crystals which diffracted to 1.9 Å resolution at the synchrotron. The presence of Sr in the crystals was detected by a fluorescence scan around the Sr *K* edge (Fig. 3). As the cryoprotection buffer in this case did not contain $SrCl_2$, this component was back-soaked; ordered Sr^{2+} ions may be present in the crystal, the anomalous signal of which could be useful for phasing of the Rab9–GDP crystal. Thus, a SAD data set was collected at the peak wavelength of 0.7697 Å (statistics not shown), but a complete MAD data set was unattainable because of considerable radiation damage to the crystal (exposure time 40 s, $\varphi = 2^\circ$). Substructure determination using *SHELXD*/*E* (Schneider & Sheldrick, 2002) in space groups $I4_1$ and $I4_122$ was unsuccessful, probably owing to the radiation damage. Current efforts focus on both the collection of a more complete data set for MAD phasing and the phasing of the data by (hitherto unsuccessful) molecular replacement using the known structures of Ypt7p (52% sequence identity; Constantinescu *et al.*, 2002), Rab5c (47% sequence identity; Merithew *et al.*, 2001), Rab3a (45% sequence identity; Dumas *et al.*, 1999; Ostermeier & Brünger, 1999) and Ypt51 (41% sequence identity; Esters *et al.*, 2000).

The authors would like to thank Uwe Müller of the Protein Structure Factory (PSF) at BESSY for guidance during data collection and Suzanne Pfeffer for providing the Rab9 cDNA. This work was supported by a grant from the SFB523 to MGR.

References

Carroll, K. S., Hanna, J., Simon, I., Krize, J., Barbero, P. & Pfeffer, S. R. (2001). *Science*, **292**, 1373–1376.
Collaborative Computational Project, Number 4 (1994). *Acta Cryst.* D**50**, 760–763.
Constantinescu, A. T., Rak, A., Alexandrov, K., Esters, H., Goody, R. S. & Scheidig, A. J. (2002). *Structure*, **10**, 569–579.
Diaz, E. & Pfeffer, S. R. (1998). *Cell*, **93**, 433–443.
Dumas, J. J., Zhu, Z., Connolly, J. L. & Lambright, D. G. (1999). *Structure Fold. Des.* **7**, 413–423.
Esters, H., Alexandrov, K., Constantinescu, A. T., Goody, R. S. & Scheidig, A. J. (2000). *J. Mol. Biol.* **298**, 111–121.
Merithew, E., Hatherly, S., Dumas, J. J., Lawe, D. C., Heller-Harrison, R. & Lambright, D. G. (2001). *J. Biol. Chem.* **276**, 13982–13988.
Ostermeier, C. & Brünger, A. T. (1999). *Cell*, **96**, 363–374.
Otwinowski, Z. & Minor, W. (1997). *Methods Enzymol.* **276**, 307–326.
Pfeffer, S. R. (2001). *Trends Cell Biol.* **11**, 487–491.
Schneider, T. R. & Sheldrick, G. M. (2002). *Acta Cryst.* D**58**, 1772–1779.
Segev, N. (2001). *Curr. Opin. Cell. Biol.* **13**, 500–511.
Tucker, J., Sczakiel, G., Feuerstein, J., John, J., Goody, R. S. & Wittinghofer, A. (1986). *EMBO J.* **5**, 1351–1358.
Vetter, I. R. & Wittinghofer, A. (2001). *Science*, **294**, 1299–1304.